Metals and Materials International (2021) 27:2977–2988
https://doi.org/10.1007/s12540-019-00606-7

Microstructure, Mechanical Properties and Fracture Behavior of Magnesium/Steel Bimetal Using Compound Casting Assisted with Hot-Dip Aluminizing

Wenming Jiang[1] · Haixiao Jiang[1] · Guangyu Li[1] · Feng Guan[1] · Junwen Zhu[1] · Zitian Fan[1]

Received: 17 October 2019 / Accepted: 30 December 2019 / Published online: 16 January 2020

Abstract
In this work, microstructure, mechanical properties and fracture behavior of the magnesium/steel bimetal using compound casting assisted with hot-dip aluminizing were investigated, and the interface bonding mechanism of the magnesium/steel bimetal were also analyzed. The results indicate that the magnesium/steel bimetal obtained without hot-dip aluminizing had larger gaps through the whole interface without reaction layers between magnesium and steel, leading to a poor mechanical bonding. After the steel substrate was hot-dip aluminized, an intermetallic layer along with an Al topcoat layer were formed on the surface of the steel substrate, and the intermetallic layer was constituted by Fe_2Al_5, τ_{10}-$Al_9Fe_4Si_3$, $FeAl_3$ and τ_6-$Al_{4.5}FeSi$ phases. In the case of the magnesium/steel bimetal obtained with hot-dip aluminizing, a compact and uniform interface layer with an average thickness of about 17 μm that consisted of Fe_2Al_5, τ_{10}-$Al_9Fe_4Si_3$, $FeAl_3$ and $Al_{12}Mg_{17}$ intermetallic compounds was formed between the magnesium and the steel, obtaining a superior metallurgical bonding. The interface layer had much higher nano-hardnesses compared to the magnesium and steel matrixes, and its average nano-hardness was up to 11.1 GPa, while there were respectively 1.1 and 4.2 GPa for the magnesium and steel matrixes. The shear strength of the magnesium/steel bimetal with hot-dip aluminizing reached to 23.3 MPa, which increased by 8.59 times than that of the composites without hot-dip aluminizing. The fracture of the magnesium/steel bimetal with hot-dip aluminizing represented a brittle fracture nature, initiating from the interface layer.

Keywords Magnesium · Steel · Bimetal · Aluminizing · Interface · Compound casting

1 Introduction

Magnesium alloys have been widely used in automotive, aerospace, military and electronic industries due to their many advantages, such as low density, high strength-to-weight ratio, superior electromagnetic shielding and damping capacity as well as good castability and workability [1–3]. However, a number of disadvantages of the magnesium alloys including low strength and hardness, poor wear, ductility and corrosion resistance greatly limit their further applications in some cases [4]. Steel is commonly employed in the industrial applications, and it possesses superior strength, hardness, wear, ductility as well as corrosion resistance compared to the magnesium alloys [5–7]. Combining the magnesium alloys and the steel to prepare the magnesium/steel bimetal may be the most potential approach for enlarging industrial applications of the magnesium alloys and steel [8].

It is well known that the joining of the magnesium alloys and the steel is always a large challenge. On the one hand, the thermal-physical properties of the magnesium alloys and the steel have larger differences, such as melting points, thermal conductivities and thermal expansion coefficients [9, 10]. Moreover, the solubility of Fe in Mg is 0.00043 at%, while the solid solubility of Mg in Fe is close to zero, in light of the Mg–Fe equilibrium phase diagram. They are immiscible even if at a liquid state; meanwhile, they do not react with each other [11, 12]. As a result, the magnesium and steel have poor wettability, and it is difficult to obtain a

✉ Wenming Jiang
wmjiang@hust.edu.cn; jwenming@163.com

✉ Zitian Fan
fanzt@hust.edu.cn

[1] State Key Lab of Materials Processing and Die and Mould Technology, Huazhong University of Science and Technology, Wuhan 430074, People's Republic of China

metallurgical bonding between the magnesium and the steel. Currently, a larger number of welding methods are used to join the magnesium and the steel, such as friction stir welding [13, 14], laser welding [15, 16], diffusion bonding [17, 18], electric resistance welding [19, 20], and ultrasonic spot welding [21, 22]. Still, it is difficult to directly achieve a metallurgical bonding between the magnesium alloy and the steel by use of the welding methods. In general, the metallurgical bonding of the magnesium and the steel is mainly obtained during the welding technologies through the addition of interlayers, coatings as well as filling wires, especially in the interlayers, such as Al [23], Cu [24], Zn [25] and Ni [26]. It is noted that the element that can interact with both of the magnesium and steel should be selected as an intermediate element. For instance, the Cu is used properly as a transition element between the magnesium and steel because the Cu can react with the Mg and Fe, thereby creates an interface layer [27]. The Zn can improve the weldability of the Mg to the steel due to the formation of the Mg–Zn product [28]. The welding methods usually prepare the magnesium/steel bimetal with a simple shape, and it is costly. And, the welding methods may leading to large welding residual stress and cracking problems. A good metallurgical bonding of the magnesium and the steel is of great importance to ensure a superior mechanical properties for the magnesium/steel bimetal. However, how to obtain an excellent metallurgical bonding between the magnesium and the steel is always a challenge.

In this work, the steel substrate was first hot-dip aluminized to prevent the surface of the steel substrate from the oxidation and to form an intermetallic layer on the surface of the steel substrate, and the magnesium/steel bimetal was then fabricated using a compound casting process. The objective of the present work is to develop a simple and economic method to prepare the magnesium/steel bimetal with a complex structure and to investigate the microstructure, mechanical properties and fracture behavior of the magnesium/steel bimetal. In addition, the interface bonding mechanism of the magnesium/steel bimetal were also discussed.

2 Experimental

2.1 Materials

The low carbon steel and AZ91D magnesium alloy were respectively chosen as a solid substrate material and a molten bath to produce the magnesium/steel bimetal, and the A356 aluminum alloy was adopted as a hot-dip aluminizing material for the low carbon steel substrate. Table 1 lists the chemical compositions of the experimental materials.

The steel substrates that had a diameter of 32 mm, a wall thickness of 3 mm and a height of 70 mm were obtained from a low carbon steel tube using a cutting machine. The steel substrates were first ground up to 2000 grit using silicon carbide papers, and they were then immersed into a 15 wt% sodium hydroxide solution at 50 °C for 20 min to remove the oil contamination on the surface of the steel substrates. Next, the steel substrates were rinsed using a 0.5 mol/l hydrochloric acid to remove the iron rust on the surface of the steel substrates, and were finally washed using the ethanol prior to drying.

2.2 Preparation Process of the Magnesium/Steel Bimetal

The AZ91D magnesium alloy ingots were melted using an electric furnace under a protective gas atmosphere of CO_2-0.5% SF_6. As the temperature of the AZ91D magnesium alloy melt reached to 730 °C, the slag of the molten metal was skimmed, and the temperature of the melt was further elevated up to 780 °C, waiting for pouring process. The A356 aluminum alloy ingots were placed inside stainless steel crucible to melt using the electric furnace, and the A356 aluminum alloy melt was refined using the argon gas at 730 °C for 15 min before slag skimming, followed by elevating the melt temperature to 770 °C. The steel substrates were first immersed into the A356 aluminum alloy melt at 770 °C for 10 min to perform the hot-dip aluminizing process. Subsequently, the steel substrates that had been hot-dip aluminized were rapidly placed inside a metal mold with a preheating temperature of 300 °C, and the AZ91D magnesium alloy molten metal with a temperature of 780 °C was then poured into the metal mold. Finally, the magnesium/steel bimetal was obtained when the liquid metal finished

Table 1 Chemical compositions of the experimental materials (wt%)

Alloys	Compositions								
	Al	Zn	Mn	Si	C	Cu	Cr	Fe	Mg
Steel	–	–	0.54	0.23	0.20	–	0.02	Bal.	–
AZ91D	9.08	0.62	0.23	0.06	–	0.028	–	–	Bal.
A356	Bal.	–	–	6.81	–	–	–	0.21	0.44

solidification. For comparison, the steel substrates without hot-dip aluminizing were also used to prepare the magnesium/steel bimetal. Figure 1 presents a schematic illustration of the present experimental device for the preparation of the magnesium/steel bimetal.

2.3 Microstructural Characterizations

The hot-dip aluminized sample was first ground and polished, and then was etched using a 0.5% hydrofluoric acid solution to observe the microstructure and analyze the chemical compositions of the hot-dip aluminized sample using a Quanta 400 scanning electron microscope (SEM) equipped with an energy-dispersive X-ray spectroscopy (EDS). An XRD-7000 X-ray diffractometer (XRD) was also used to identify the phase compositions of the hot-dip aluminized sample. In order to display the gaps between the magnesium and the steel, the cross-sections of the magnesium/steel bimetal were first permeated using a penetrating agent, and they were then stained to red using an imaging agent, and the macro-characterizations of the magnesium/steel bimetal were finally observed using a super depth microscope. If the cross-sections of the magnesium/steel bimetal show red, it indicates that there are gaps and pores defects in the samples. The metallographic samples of the magnesium/steel bimetal were etched using a 4% nital solution after grinding and polishing, and the interfacial microstructures were then observed by an OLYMPUS-MG3 metallographic microscope and the SEM, and the EDS analysis method was used to analyze the phase compositions at the interface of the bimetal.

2.4 Mechanical Properties

The nano-hardnesses across the interfaces of the magnesium/steel bimetallic samples were measured with a TI 750 nano-mechanical test instrument, and the test force and holding time were 6000 μN and 15 s, respectively.

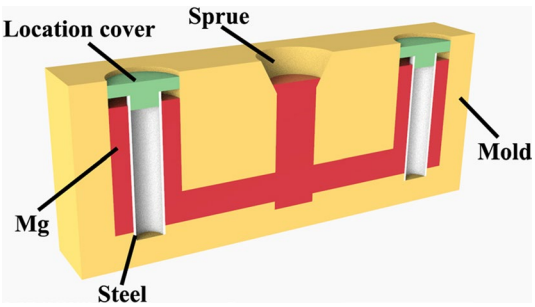

Fig. 1 Schematic illustration of the experimental device for the preparation of the magnesium/steel bimetal

The push-out test was used to measure the bonding strength of the magnesium/steel bimetal using a ZwickZ1000 universal testing machine [29, 30], and the indenter moving rate was 0.5 mm/min in this work. At least three samples were measured to ensure the repeatability. Afterwards, the XRD, SEM, EDS as well as the metallographic microscope were applied to analyze the fracture behavior of the magnesium/steel bimetal.

3 Results

3.1 Microstructure and Composition of the Steel Substrate with Hot-Dip Aluminizing

Figure 2 exhibits SEM micrographs and EDS analysis of the steel substrate with hot-dip aluminizing. It is obvious that a compact and uniform Al coating as an intermetallic layer is observed on the surface of the steel substrate, and the residual Al as a topcoat is covered on the surface of the Al coating, as shown in Fig. 2a, b. As can be seen from Fig. 2c, it indicates that the Al, Si and Fe elements evidently diffuse in the Al coating layer, particularly in the Al and Fe elements. Table 2 presents EDS analysis results of the points indicated in Fig. 2b. In light of the EDS results, Al–Fe binary system [31, 32] as well as the Al–Fe–Si ternary system [33, 34], it can be revealed that the topcoat layer is mainly composed of Al, deriving from the A356 aluminum alloy melt during the hot-dip aluminizing process, and the Al coating consists of τ_6-$Al_{4.5}FeSi$, $FeAl_3$, τ_{10}-$Al_9Fe_4Si_3$ and Fe_2Al_5 phases successively from the topcoat layer side to the steel substrate side. In addition to the EDS analysis, the phase identification of the Al coating was also performed using the XRD analysis, as shown in Fig. 3, and the XRD analysis results further confirm the existences of the τ_6-$Al_{4.5}FeSi$, $FeAl_3$, τ_{10}-$Al_9Fe_4Si_3$ and Fe_2Al_5 phases in the Al coating.

3.2 Interfacial Characterizations of the Magnesium/Steel Bimetal

Figure 4 shows photos of the magnesium/steel bimetals obtained with and without hot-dip aluminizing. As can be seen from Fig. 4a, a large number of gaps exhibiting red with a continuous distribution are present at the interface of the magnesium/steel bimetallic composite without hot-dip aluminizing, suggesting that a poor bonding of the magnesium and steel is obtained. In comparison, the interface of the magnesium/steel bimetallic composite with hot-dip aluminizing is compact, which is almost absent from the gaps, showing a superior bonding between the magnesium and the steel, as shown in Fig. 4b.

The optical micrographs of the interfaces of the magnesium/steel bimetals obtained with and without hot-dip

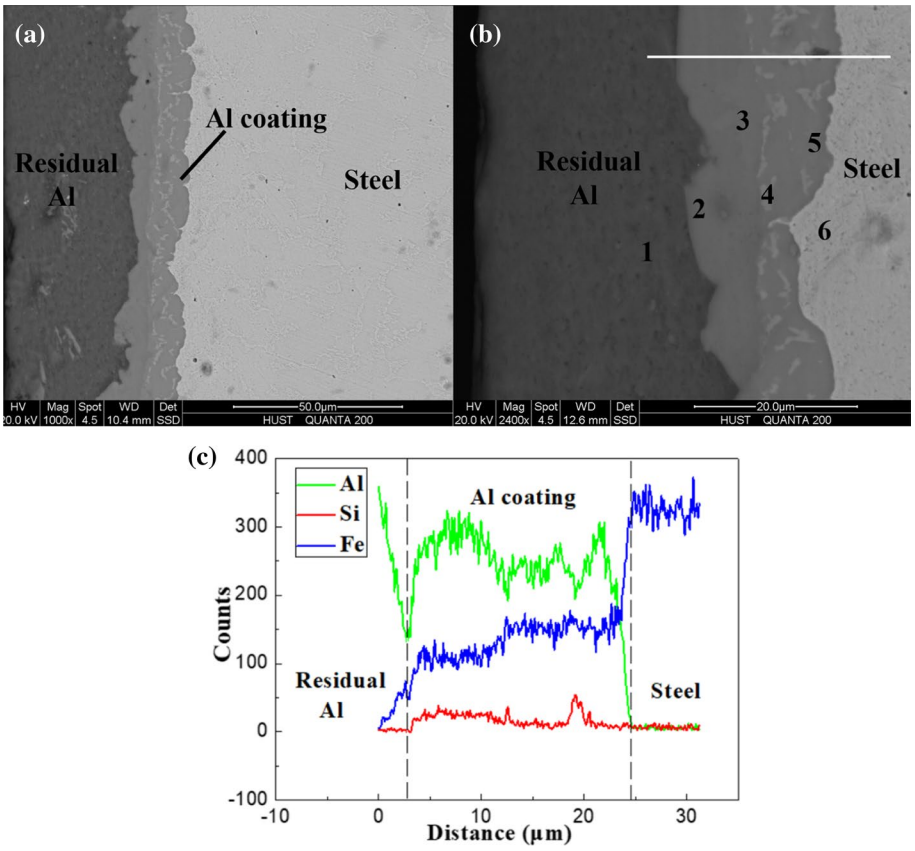

Fig. 2 SEM micrographs and EDS analysis of the steel substrate with hot-dip aluminizing: **a**, **b** SEM micrographs, **c** EDS line scan

Table 2 EDS analysis results of the points indicated in Fig. 2b

Number	Element compositions (at%)				Inference component
	Al	Fe	Si	Mg	
1	97.20	–	2.46	0.34	Al
2	69.55	19.03	11.42	–	τ_6-$Al_{4.5}FeSi$
3	69.82	25.48	04.70	–	$FeAl_3$
4	53.04	35.53	11.43	–	τ_{10}-$Al_9Fe_4Si_3$
5	68.70	28.82	2.48	–	Fe_2Al_5
6	–	100.00	–	–	Fe

aluminizing are displayed in Fig. 5. It is found that the gap with an average width of about 29 μm is observed through the whole interface of the magnesium/steel bimetallic composite without hot-dip aluminizing, and no any metallurgical layer at the interface is generated, showing a poor bonding between the magnesium and the steel, as shown in Fig. 5a. In contrast, a uniform and compact interface with an average thickness of approximately 17 μm is formed between the magnesium and the steel in the case of the hot-dip aluminizing, as shown in Fig. 5b. Therefore, the hot-dip aluminizing significantly improves the interface bonding of the magnesium/steel bimetal.

In order to further investigate interfacial characterizations of the magnesium/steel bimetals obtained with and without

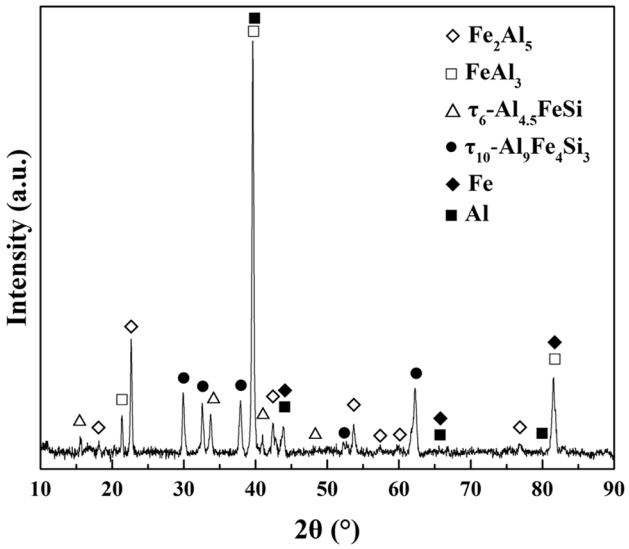

Fig. 3 XRD patterns of the steel substrate with hot-dip aluminizing

hot-dip aluminizing, the high magnification SEM micrographs and EDS analyses of the interfaces were carried out in the present work, as shown in Fig. 6. Without the application of the hot-dip aluminizing, the interface of the magnesium/steel bimetallic composite has an evident large gap, as shown in Fig. 6a, which is in good agreement with the

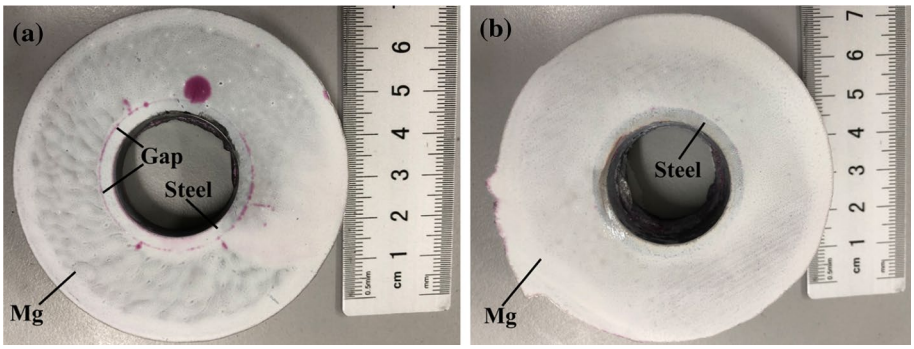

Fig. 4 Photos of the magnesium/steel bimetals obtained with and without hot-dip aluminizing: **a** without hot-dip aluminizing, **b** with hot-dip aluminizing

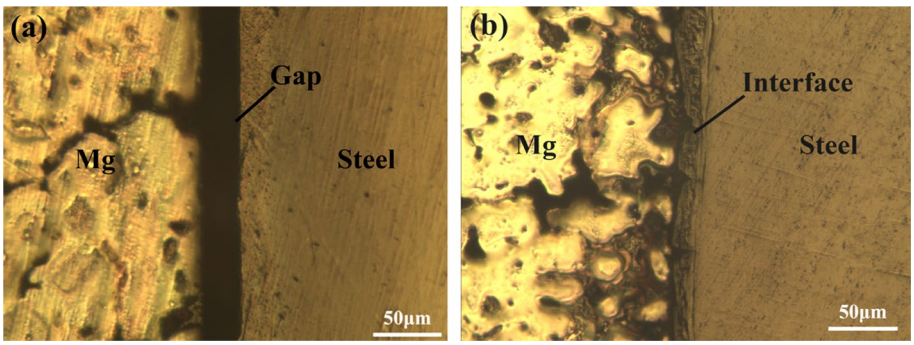

Fig. 5 Optical micrographs of the interfaces of the magnesium/steel bimetals obtained with and without hot-dip aluminizing: **a** without hot-dip aluminizing, **b** with hot-dip aluminizing

results of the macro-characteristic and optical micrograph of the magnesium/steel bimetallic composite, exhibiting a poor interface bonding. Figure 6b shows the EDS line scan of the interface corresponding to Fig. 6a. According to Fig. 6b, it is clear that there are no any diffusions at the interface of the magnesium and steel, indicating that the magnesium and steel have no metallurgical bonding. By comparison, a uniform and compact interface layer is formed between the magnesium and the steel with the application of the hot-dip aluminizing, as shown in Fig. 6c. More higher magnification SEM micrograph of the interface corresponding to Fig. 6c shows that the interface layer is free from pore and gap, and it is well combined with the magnesium and steel matrixes, as shown in Fig. 6d. Moreover, the interface layer close to the magnesium matrix exhibits a sawtooth morphology, while it displays a flat morphology adjacent to the steel matrix. The EDS line scan and map scan analyses of the interface obtained with hot-dip aluminizing demonstrate that the Al, Fe, Mg and Si elements have obvious diffusions at the interface between the magnesium and the steel, as shown in Fig. 6e, f, implying that the metallurgical bonding has occurred when the hot-dip aluminizing process was adopted. The EDS analysis method was used to further investigate the chemical compositions of the interface layer, and Table 3 represents the EDS analysis results of the interface layer corresponding to the points indicated in Fig. 6d. As can be seen, the interfacial microstructure is mainly composed of elongated crystals close to the magnesium matrix. Depending on the results of the EDS analysis and the Al–Mg binary phase diagram [35–37], as shown in Fig. 7, the elongated crystals are confirmed to be the $Al_{12}Mg_{17}$ phase, exhibiting an irregular distribution at the interface. In addition to the $Al_{12}Mg_{17}$ phase, the interface layer is constituted by the $FeAl_3$, τ_{10}-$Al_9Fe_4Si_3$ and Fe_2Al_5 phases, which successively distribute from the $Al_{12}Mg_{17}$ phase side to the steel matrix side. Therein, the white phase with a thin thickness in the interface layer is the τ_{10}-$Al_9Fe_4Si_3$ intermetallic compound, which primarily shows a banded distribution parallel to the interface layer. While, the grey phases with a plate shape are the $FeAl_3$ and Fe_2Al_5 intermetallic compounds, and they have evidently wider thicknesses in comparison with the τ_{10}-$Al_9Fe_4Si_3$ phase. Furthermore, compared the interfacial microstructure of the Al coating on the surface of the steel substrate during the hot-dip aluminizing process, it is found that the τ_6-$Al_{4.5}FeSi$ phase has disappeared at the interface layer of the magnesium/steel bimetal.

Through the above investigations, it can be noted that the hot-dip aluminizing obviously improves the interface bonding of the magnesium/steel bimetal, resulting in a uniform and compact metallurgical interface between the magnesium and the steel, which is constituted by the Fe_2Al_5, τ_{10}-$Al_9Fe_4Si_3$, $FeAl_3$ and $Al_{12}Mg_{17}$ intermetallic phases.

3.3 Mechanical Properties of the Magnesium/Steel Bimetal

Figure 8 shows the nano-hardness profile across the interface of the magnesium/steel bimetal obtained with hot-dip

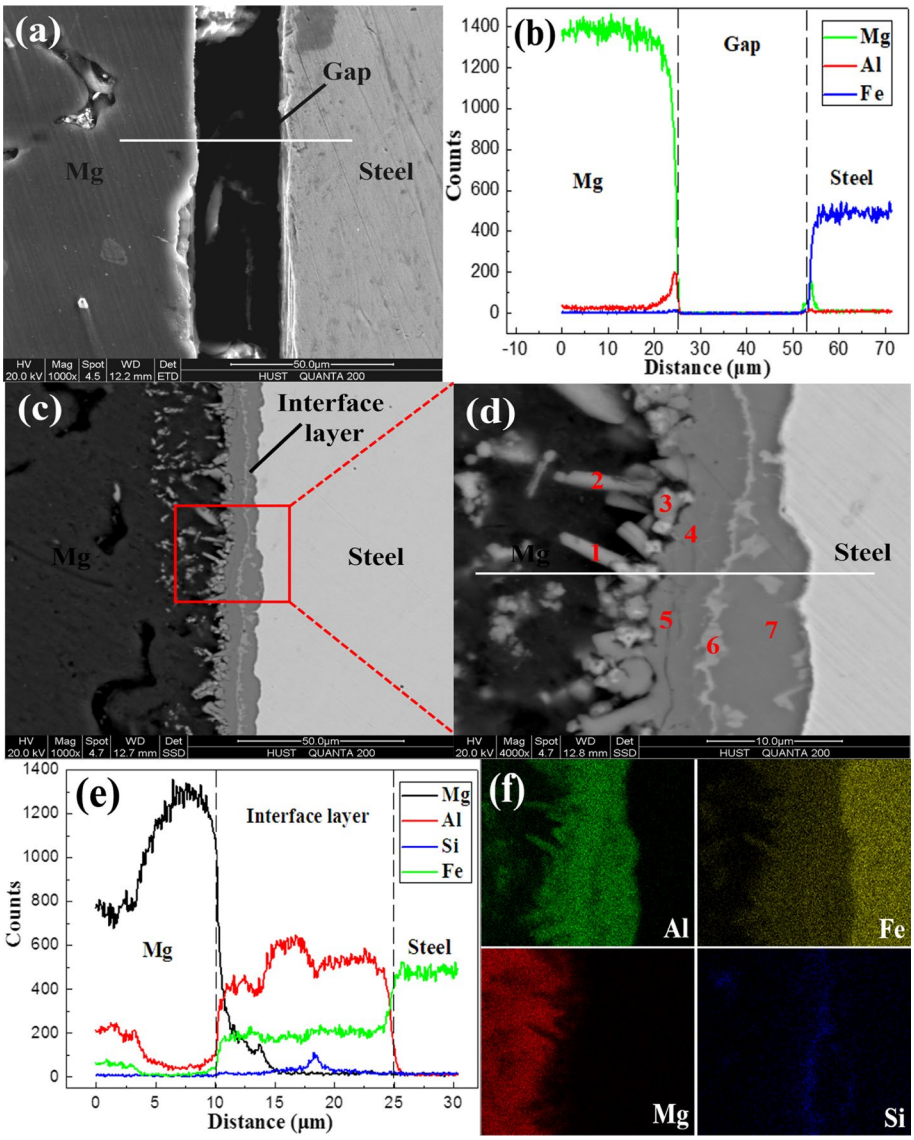

Fig. 6 SEM micrographs and EDS analyses of the interfaces of the magnesium/steel bimetals obtained with and without hot-dip aluminizing: **a**, **b** SEM micrograph and EDS line scan of the interface without hot-dip aluminizing, respectively, **c**, **d** SEM micrographs of the interface with hot-dip aluminizing, **e** EDS line scan of the interface with hot-dip aluminizing corresponding to **d**, **f** EDS maps of the interface with hot-dip aluminizing corresponding to **d**

Table 3 EDS analysis results of the interface corresponding to the points indicated in Fig. 6d

Number	Element compositions (at%)				Inference component
	Al	Fe	Si	Mg	
1	45.69	12.59	01.62	40.10	$Al_{12}Mg_{17}$
2	45.69	14.46	01.01	38.84	$Al_{12}Mg_{17}$
3	39.35	12.12	01.45	47.07	$Al_{12}Mg_{17}$
4	67.49	26.08	06.44	–	$FeAl_3$
5	65.98	26.21	07.81	–	$FeAl_3$
6	50.58	33.27	16.15	–	τ_{10}-$Al_9Fe_4Si_3$
7	70.37	27.99	01.64	–	Fe_2Al_5

aluminizing. It can be seen that the interface layer has much higher nano-hardnesses compared to the magnesium and steel matrixes, especially for the magnesium matrix, and the average nano-hardnesses of the interface layer, magnesium and steel matrixes are respectively 11.1, 1.1 and 4.2 GPa. The above results also suggest that the metallurgical interface between the magnesium and the steel has generated. In addition, the nano-hardnesses of the interface exhibit a slight decrease from the magnesium matrix side toward the steel matrix side.

Figure 9 demonstrates the shear strengths of the magnesium/steel bimetals obtained with and without hot-dip aluminizing. The push-out response curves indicate that a nearly linear loading first takes place prior to the drop of an abrupt load, obtaining a maximum load, and a frictional sliding finally occurs, in accordance with the findings of other reports [38, 39]. It is obvious that the magnesium/steel bimetallic composite obtained with hot-dip aluminizing has a remarkably higher shear strength than the composite obtained without hot-dip aluminizing, mainly as a result of

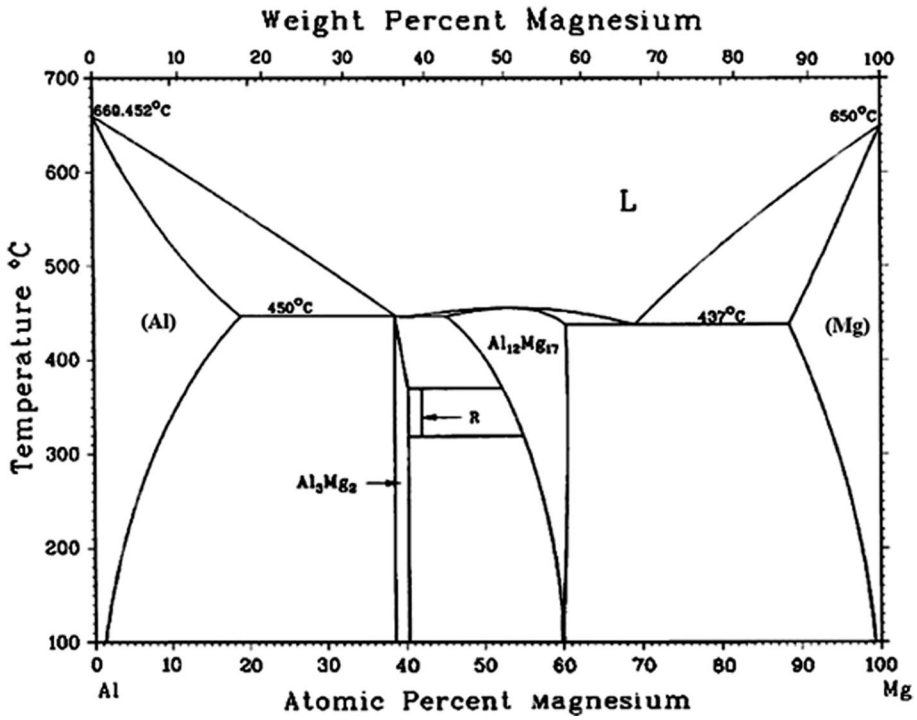

Fig. 7 Al–Mg binary phase diagram

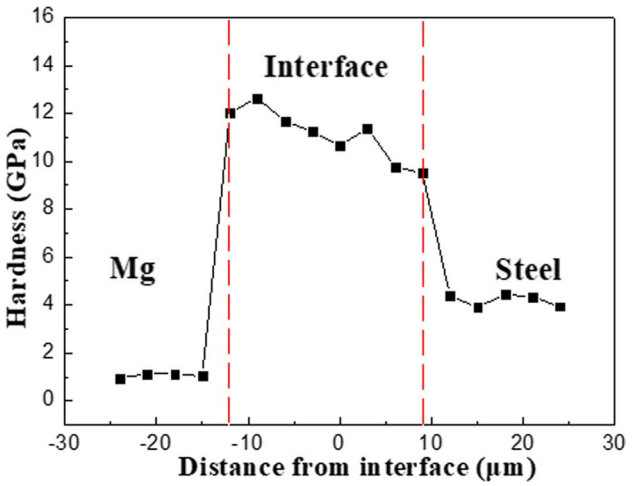

Fig. 8 Nano-hardness profile across the interface of the magnesium/steel bimetal obtained with hot-dip aluminizing

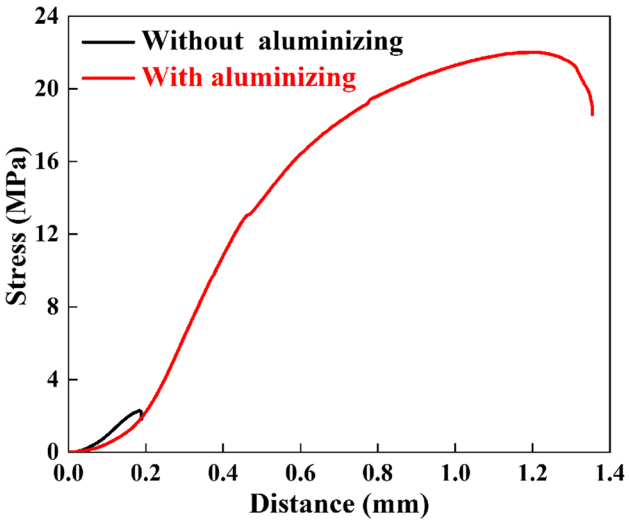

Fig. 9 Shear strengths of the magnesium/steel bimetals obtained with and without hot-dip aluminizing

its superior metallurgical bonding. The shear strength of the magnesium/steel bimetallic composite obtained with hot-dip aluminizing reaches to 23.3 MPa, which increases by 8.59 times compared to that of the composite obtained without hot-dip aluminizing. Thus, the hot-dip aluminizing significantly enhances the interface bonding of the magnesium/steel bimetal.

Figure 10 shows the shear fracture morphologies of the magnesium/steel bimetals obtained with and without hot-dip aluminizing, and the EDS analysis results of the shear-fractured samples corresponding to Fig. 10 are listed in Table 4.

It can be observed that the fracture surface of the shear sample without hot-dip aluminizing displays a completely flat morphology without any transformations, as shown in Fig. 10a. The EDS results reveal that no any intermetallic phases are detected in the fractured surface without hot-dip aluminizing, and only the composition of the steel substrate is found, as shown in Fig. 10b, and it means that only a sliding debonding between the magnesium and the steel occurs during the push-out test process. In the fractured surface of the magnesium/steel bimetallic composite with hot-dip

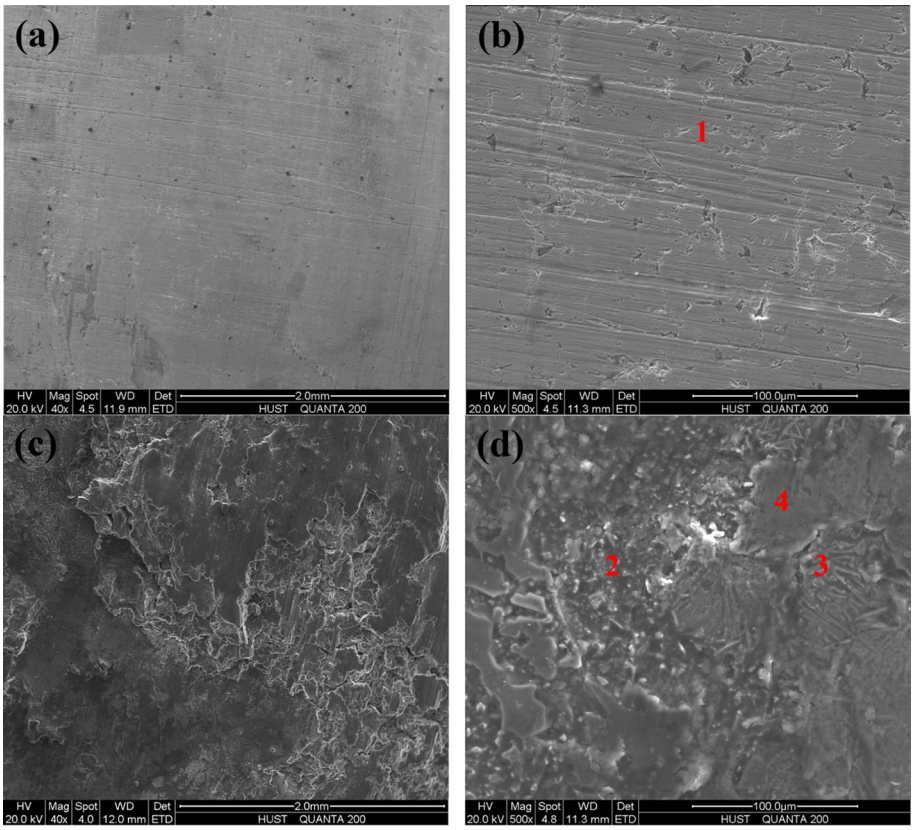

Fig. 10 SEM micrographs of the shear-fractured magnesium/steel bimetals obtained with and without hot-dip aluminizing: **a**, **b** without hot-dip aluminizing, **c**, **d** with hot-dip aluminizing

Table 4 EDS analysis results of the shear-fractured samples obtained with and without hot-dip aluminizing

Number	Element compositions (at%)					Inference component
	Al	Fe	Si	Mg	O	
1	–	90.59	–	05.72	03.69	Fe
2	46.44	–	–	53.56	–	$Al_{12}Mg_{17}$
3	69.39	20.45	04.01	06.15		$FeAl_3$
4	07.08	–	–	92.92		Mg

aluminizing, a brittle fracture morphology with some flat planes and transformations is observed, while the fractured surface is rough compared to that of the sample without hot-dip aluminizing, as shown in Fig. 10c. According to the EDS results of the fractured surface, it notes that the fracture of the magnesium/steel bimetallic composite with hot-dip aluminizing mainly initiates with the intermetallic phases in the interface layer between the magnesium and the steel, such as the $Al_{12}Mg_{17}$, $FeAl_3$ phases, and many crushed particles are found in the fracture surface, as shown in Fig. 10d. As the $Al_{12}Mg_{17}$ and $FeAl_3$ intermetallic compounds belong to the hard and brittle phases, they are easy to crack in the interface layer when they are loaded [40]. Consequently, the crack propagation path of the shear fracture preferentially passes through these intermetallic phases in the interface layer. Furthermore, the Mg is also detected resulting from the peeling during the frictional sliding process.

Additionally, the fractured surface of the magnesium/steel bimetallic composite with hot-dip aluminizing was further analyzed using the XRD analysis method, and Fig. 11 illustrates the XRD patterns of the fractured surface. As can be seen, the XRD analysis result also proves that the $Al_{12}Mg_{17}$, $FeAl_3$, Fe_2Al_5 phases are present in the fractured surface, indicating that the fracture of the magnesium/steel bimetallic composite with hot-dip aluminizing primarily takes place in the interface layer.

Figure 12 exhibits metallographs of the side views of the fractured magnesium/steel bimetals obtained with and without hot-dip aluminizing in order to reveal the fracture locations for different samples. As demonstrated in Fig. 12a, b, it is evident that the side view of the fractured surface of the sample without hot-dip aluminizing is very straight, and only the steel substrate can be observed, without any interface layers on the fractured surface, and

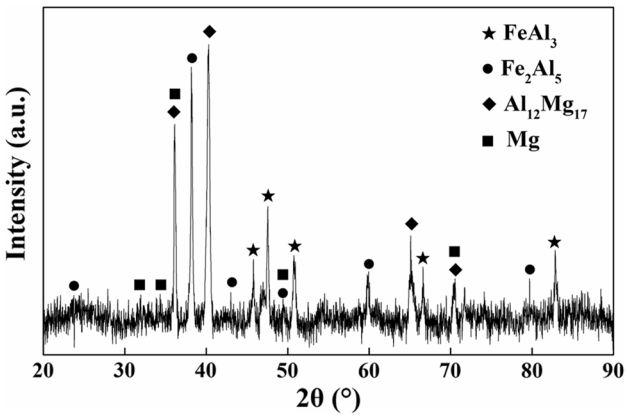

Fig. 11 XRD patterns of the fractured magnesium/steel bimetal obtained with hot-dip aluminizing

it means that the fracture of the sample without hot-dip aluminizing primarily initiates from the gap between the magnesium and the steel, leading to a poor bonding strength. While the side view of the fractured surface of the sample with hot-dip aluminizing is very curve, and an interface layer is obviously observed on the fractured surface, as shown in Fig. 12c, d, indicating that the fracture of the magnesium/steel bimetallic composite with hot-dip aluminizing mainly occurs in the interface layer, which is consistent with the results of the shear fracture morphologies and XRD patterns, resulting in the enhancement of the bonding strength.

4 Discussion

In this study, the interface bonding mechanism of the magnesium/steel bimetal are proposed as follows. In the case of the magnesium/steel bimetal obtained without hot-dip aluminizing, the wettability of the magnesium and steel is very poor due to their larger differences in the thermal physics properties. And, the solubility between magnesium and iron is extremely small, and no any intermetallic compounds are formed between the magnesium and the iron, according to the Mg–Fe binary phase diagram (Fig. 13) [41]. What is more, the steel is tend to oxidize, thereby generates the oxide film on the surface of the steel substrate, preventing a direct contact of the magnesium melt and the steel substrate. The magnesium melt is difficult to spread on the surface of the steel substrate. As a consequence, the larger gaps in the interface of the magnesium/steel bimetal without hot-dip aluminizing are formed, and the reaction layer between the magnesium and steel is not generated, leading to a poor mechanical bonding.

During the hot-dip aluminizing process, when the steel substrate is immersed into the molten aluminum bath, the Al, Si and Fe elements from the molten aluminum bath and the steel substrate begin to inter-diffuse under a high heat capacity of the molten aluminum. The complex diffusion reactions occur among the Al, Fe and Si elements, generating a continuous metallic transition on the surface of the steel substrate. Because the Fe_2Al_5 intermetallic phase has a low activation energy and 30% vacancy rate in

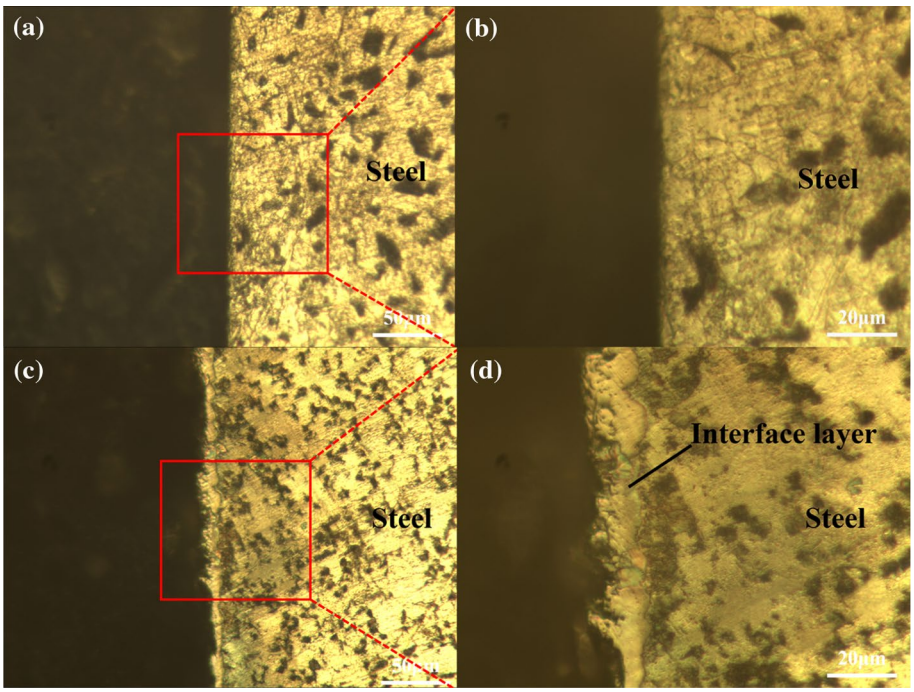

Fig. 12 Optical micrographs of the side views of the fractured magnesium/steel bimetals obtained with and without hot-dip aluminizing: **a**, **b** without hot-dip aluminizing, **c**, **d** with hot-dip aluminizing

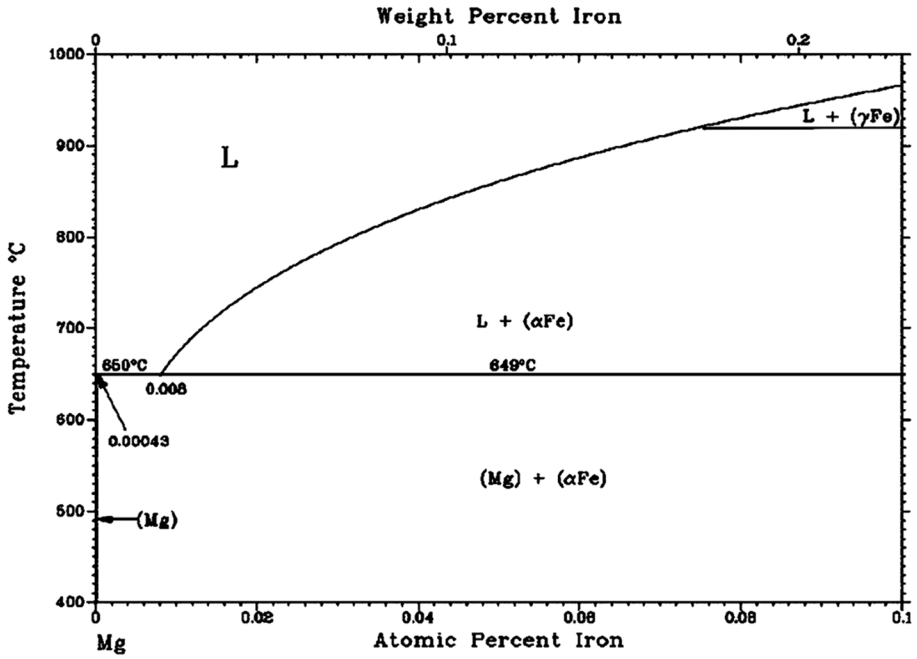

Fig. 13 Mg–Fe binary phase diagram

the c-axis of the crystal structure, it makes the Al atoms to diffuse much more rapidly inward, resulting in the preferential growth of the Fe_2Al_5 phase along the diffusion direction adjacent to the steel substrate [42]. Meanwhile, the Fe_2Al_5 intermetallic phase also obtains a larger fraction in the reaction layer. With the further process of the diffusion reaction, other intermetallic compounds may generate according to the following reactions [43–46].

$$Fe_2Al_5 + Al \rightarrow FeAl_3 \tag{1}$$

$$L + FeAl_3 \rightarrow \tau_5 + (Al) \tag{2}$$

$$\tau_1 + \tau_3 + \tau_{11} \rightarrow \tau_{10} \tag{3}$$

$$L + \tau_5 \rightarrow (Al) + \tau_6 \tag{4}$$

$$L \rightarrow (Al) + (Si) + \tau_6 \tag{5}$$

where τ_1, τ_3, τ_5, τ_6, τ_{10} and τ_{11} represent respectively $Al_2Fe_2Si_3$, Al_2FeSi, Al_8Fe_2Si, $Al_{4.5}FeSi$, $Al_9Fe_4Si_3$ and Al_5Fe_2Si phases [47, 48]. As a result, an intermetallic layer is formed on the surface of the steel substrate, which is constituted by the Fe_2Al_5, τ_{10}-$Al_9Fe_4Si_3$, $FeAl_3$ and τ_6-$Al_{4.5}FeSi$ phases successively from the steel substrate side to the topcoat layer side. The topcoat layer that is located in the outermost layer consists of the Al, as shown in Fig. 2. Here, it should be pointed out that the formation of the intermetallic phases during the hot-dip aluminizing process may be determined by many factors, such as hot-dip aluminizing temperature and time, chemical potentials, nucleation conditions, surface roughness of the substrates, and compositions of the alloys [47, 49].

For the case of the magnesium/steel bimetal prepared with hot-dip aluminizing, the steel substrate has obtained an intermetallic layer along with an Al topcoat layer prior to the pouring process. Thus, the wettability between the magnesium and the steel is significantly improved, and the oxidation of the steel substrate can be also avoided, and the liquid magnesium spreads more easily on the surface of the steel substrate. Figure 14 draws a schematic illustration of the metallurgical interface formation of the magnesium/steel bimetal obtained with hot-dip aluminizing. Once the steel substrate with an intermetallic layer and an Al topcoat layer contacts with the molten magnesium melt, the Al topcoat layer first is fused under the high heat capacity of the magnesium melt. Simultaneously, the τ_6-$Al_{4.5}FeSi$ intermetallic phase close to the Al topcoat layer may be also melted under a relatively long time high heat capacity, resulting in the dissolution of the Al, Fe and Si elements in the magnesium melt, especially more Al atoms, as shown in Fig. 14b, c. Because the affinity of the Al with the magnesium is much larger than that of the Al with the Fe, and the Al and magnesium have more similar melting points, the Al and magnesium will preferentially react to form the $Al_{12}Mg_{17}$ intermetallic compound attached to the $FeAl_3$ phase in the intermetallic layer, displaying an elongated crystal morphology, as shown in Fig. 14d. Finally, an interface layer that consists of the Fe_2Al_5, τ_{10}-$Al_9Fe_4Si_3$, $FeAl_3$ and $Al_{12}Mg_{17}$ intermetallic compounds is formed between the magnesium and the steel, obtaining a superior metallurgical bonding,

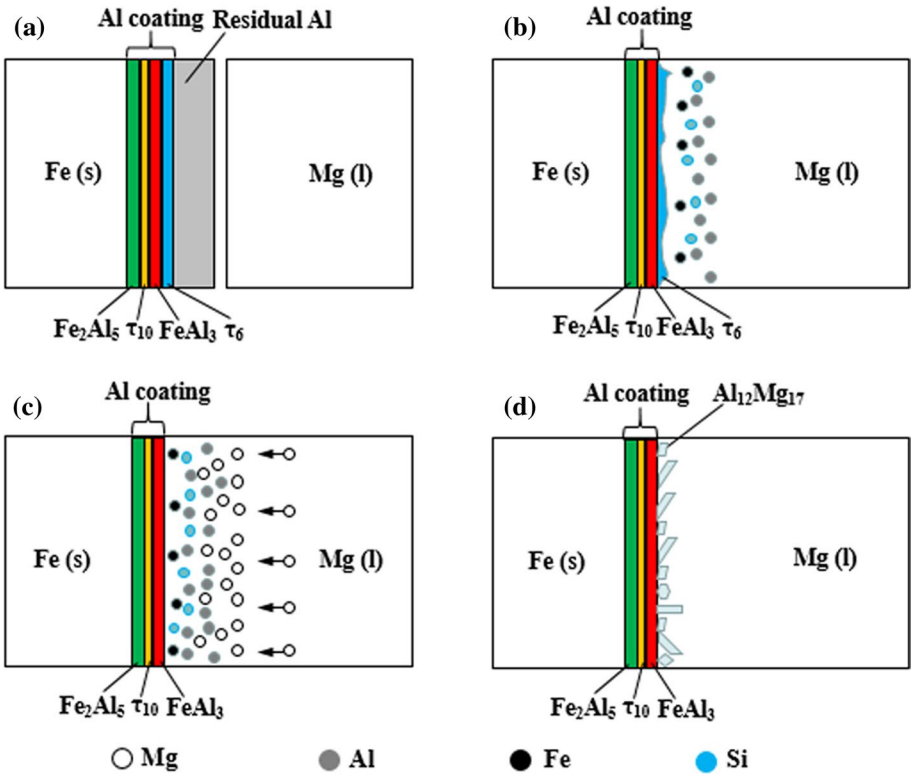

Fig. 14 Schematic illustration of the metallurgical interface bonding of the magnesium/steel bimetal obtained with hot-dip aluminizing: **a** Before pouring, **b** Residual Al and τ6 layer melting, **c** Atoms diffusing, **d** $Al_{12}Mg_{17}$ layer forming

thereby significantly improves the bonding strength of the magnesium/steel bimetal. Therefore, the hot-dip aluminizing plays an important role in enhancing the interface bonding of the magnesium/steel bimetal. Here, it should be pointed out that although the metallurgical interface remarkably increases the bonding strength of the magnesium/steel bimetal in comparison with the mechanical bonding with the gap, the high hardness $Al_{12}Mg_{17}$ and $FeAl_3$ intermetallic compounds are generally not desirable in the interface. Consequently, our future work will focus on how to avoid the brittleness and high hardness intermetallic phases in the interface, aiming at further improvement of the bonding strength of the magnesium/steel bimetal.

5 Conclusions

(1) Without hot-dip aluminizing, the larger gaps were presented through the whole interface of the magnesium/steel bimetal, and no reaction layer between the magnesium and the steel was generated, leading to a poor mechanical bonding.

(2) After the steel substrate was hot-dip aluminized, a compact and uniform intermetallic layer was formed on the surface of the steel substrate, which was constituted by the Fe_2Al_5, τ_{10}-$Al_9Fe_4Si_3$, $FeAl_3$ and τ_6-$Al_{4.5}FeSi$ phases successively from the steel substrate side to the Al topcoat layer side.

(3) In the case of the magnesium/steel bimetal obtained with hot-dip aluminizing, a compact and uniform interface layer with an average thickness of approximately 17 μm that consisted of the Fe_2Al_5, τ_{10}-$Al_9Fe_4Si_3$, $FeAl_3$ and $Al_{12}Mg_{17}$ intermetallic compounds was formed between the magnesium and the steel, obtaining a superior metallurgical bonding.

(4) The interface layer had much higher nano-hardnesses compared to the magnesium and steel matrixes, and the average nano-hardnesses of the interface layer, magnesium and steel matrixes were respectively 11.1, 1.1 and 4.2 GPa.

(5) The shear strength of the magnesium/steel bimetal obtained with hot-dip aluminizing reached to 23.3 MPa, which increased by 8.59 times in comparison with that of the composites without hot-dip aluminizing. The fracture of the magnesium/steel bimetal with hot-dip aluminizing represented a brittle fracture nature, taking place in the interface layer.

Acknowledgements This work described in this paper was financially supported by the National MCF Energy R&D Program (No. 2018YFE0313300) and the National Natural Science Foundation of China (No. 51775204), and the Natural Science Foundation of Hubei Province, China (No. 2017CFB488). The authors would also like to thank the support of the Research Project of State Key Laboratory of Materials Processing and Die and Mould Technology and the Analytical and Testing Center, HUST.

References

1. T. Lee, M. Yamasaki, Y. Kawamura, J. Go, S.H. Park, Met. Mater. Int. **25**, 372–380 (2019)
2. W.J. Kim, K.H. Han, Y.J. Lee, H. Kim, E.K. Lee, Met. Mater. Int. **24**, 720–729 (2018)
3. W.M. Jiang, G.Y. Li, Z.T. Fan, L. Wang, F.C. Liu, Metall. Mater. Trans. A **47**, 2462–2470 (2016)
4. Y.J. Kim, S.-H. Kim, J.U. Lee, J.O. Choi, H.S. Kim, Y.M. Kim, Y. Kim, S.H. Park, Mater. Sci. Eng. A **708**, 405–410 (2017)
5. Z.S. Yao, G. Xu, Z.Y. Jiang, J.Y. Tian, Q. Yuan, H.W. Ma, Met. Mater. Int. **25**, 1151–1160 (2019)
6. J.I. Yoon, J. Jung, H.H. Lee, J.Y. Kim, H.S. Kim, Met. Mater. Int. **25**, 1161–1169 (2019)
7. W.M. Jiang, G.Y. Li, Y. Wu, X.W. Liu, Z.T. Fan, J. Mater. Process. Technol. **258**, 239–250 (2018)
8. J. Cheng, J.H. Zhao, J.Y. Zhang, Y. Guo, K. He, J.J. Shangguan, F.L. Wen, Materials **12**, 1–14 (2019)
9. V.K. Patel, S.D. Bhole, D.L. Chen, Mater. Des. **45**, 236–240 (2013)
10. L. Liu, X. Qi, Z. Wu, Mater. Lett. **64**, 89–92 (2010)
11. A.M. Nasiri, P. Chartrand, D.C. Weckman, N.Y. Zhou, Metall. Mater. Trans. A **44**, 1937–1946 (2013)
12. G. Song, J.W. Yu, T.T. Li, J.F. Wang, L.M. Liu, J. Manuf. Process. **31**, 131–138 (2018)
13. S. Jana, Y. Hovanski, G.J. Grant, Metall. Mater. Trans. A **41**, 3173–3182 (2010)
14. Y.N. Wei, J.L. Li, J.T. Xiong, F. Huang, F.S. Zhang, Mater. Des. **33**, 111–114 (2012)
15. L.Q. Li, C.W. Tan, Y.B. Chen, W. Guo, C.X. Mei, J. Mater. Process. Technol. **213**, 361–375 (2013)
16. L. Li, C. Tan, Y. Chen, W. Guo, C. Mei, X. Hu, Metall. Mater. Trans. A **43**, 4740–4754 (2012)
17. W.M. Elthalabawy, T.I. Khan, Mater. Charact. **61**, 703–712 (2010)
18. W. Elthalabawy, T. Khan, J. Mater. Sci. Technol. **27**, 22–28 (2011)
19. L. Liu, L. Xiao, D.L. Chen, J.C. Feng, S. Kim, Y. Zhou, Mater. Des. **45**, 336–342 (2013)
20. Y. Feng, Y. Li, Z. Luo, Z. Ling, Z. Wang, J. Mater. Process. Technol. **236**, 114–122 (2016)
21. V.K. Patel, S.D. Bhole, D.L. Chen, J. Mater. Process. Technol. **214**, 811–817 (2014)
22. M. Shakil, N.H. Tariq, M. Ahmad, M.A. Choudhary, J.I. Akhter, S.S. Babu, Mater. Des. **55**, 263–273 (2014)
23. C.W. Tan, B. Chen, X.G. Song, L. Zhou, S.H. Meng, L.Q. Li, J.C. Feng, Weld. J. **95**, 384–394 (2016)
24. M. Ding, S.S. Liu, Y. Zheng, Y.C. Wang, H. Li, W.Q. Xing, X.Y. Yu, P. Dong, Mater. Des. **88**, 375–383 (2015)
25. R. Cao, H.X. Zhu, Q. Wang, C. Dong, Q. Lin, J.H. Chen, Mater. Sci. Technol. **32**, 1805–1817 (2016)
26. A.M. Nasiri, M.Y. Lee, D.C. Weckman, Y. Zhou, Metall. Mater. Trans. A **455**, 749–5766 (2014)
27. Y.G. Miao, D.F. Han, X.F. Xu, B.T. Wu, Mater. Charact. **93**, 87–93 (2014)
28. Y.C. Chen, K. Nakata, Mater. Des. **30**, 3913–3919 (2009)
29. M. Sacerdote-Peronnet, E. Guiot, F. Bosselet, O. Dezellus, D. Rouby, J.C. Viala, Mater. Sci. Eng., A **445–446**, 296–301 (2007)
30. W.M. Jiang, Z.T. Fan, G.Y. Li, C. Li, J. Alloys Compd. **678**, 249–257 (2016)
31. U.R. Kattner, T.B. Massalski, *Binary alloy phase diagrams* (ASM International, Material Park, 1990)
32. W.M. Jiang, Z.T. Fan, C. Li, J. Mater. Process. Technol. **226**, 25–31 (2015)
33. N. Krendelsberger, F. Weitzer, J.C. Schuster, Metall. Mater. Trans. A **38**, 1681–1691 (2007)
34. Y. Lia, P. Ochin, A. Quivy, P. Telolahy, B. Legendre, J. Alloys Compd. **298**, 198–202 (2000)
35. H. Zhang, Y.Q. Chen, A.A. Luo, Scr. Mater. **86**, 52–55 (2014)
36. J.C. Liu, J. Hu, X.Y. Nie, H.X. Li, Q. Du, J.S. Zhang, L.Z. Zhuang, Mater. Sci. Eng., A **635**, 70–76 (2015)
37. W.M. Jiang, Z.T. Fan, G.Y. Li, L. Yang, X.W. Liu, Metall. Mater. Trans. A **47**, 6487–6497 (2016)
38. O. Dezellus, M. Zhe, F. Bosselet, D. Rouby, J.C. Viala, Mater. Sci. Eng., A **528**, 2795–2803 (2011)
39. Z.L. Jiang, Z.T. Fan, W.M. Jiang, G.Y. Li, Y. Wu, F. Guan, H.X. Jiang, J. Mater. Process. Technol. **261**, 149–158 (2018)
40. G.Y. Li, W.M. Jiang, W.C. Yang, Z.L. Jiang, F. Guan, H.X. Jiang, Z.T. Fan, Metall. Mater. Trans. A **50**, 1076–1090 (2019)
41. D.X. Ren, L.M. Liu, Mater. Des. **59**, 369–376 (2014)
42. R.W. Richards, R.D. Jones, P.D. Clements, H. Clarke, Int. Mater. Rev. **39**, 191–212 (1994)
43. H. Ma, G.L. Qin, L.Y. Wang, X.M. Meng, L. Chen, Mater. Des. **90**, 330–339 (2016)
44. W.M. Jiang, Z.T. Fan, G.Y. Li, X.W. Liu, F.C. Liu, J. Alloys Compd. **688**, 742–751 (2016)
45. S. Basak, H. Das, T.K. Pal, M. Shome, Mater. Charact. **112**, 229–237 (2016)
46. Y. Du, J.C. Schuster, Z.K. Liu, R.X. Hu, P. Nash, W.H. Sun, W.W. Zhang, J. Wang, L.J. Zhang, C.Y. Tang, Z.J. Zhu, S.H. Liu, Y.F. Ouyang, W.Q. Zhang, N. Krendelsberger, Intermetallics **16**, 554–570 (2008)
47. H. Springer, A. Kostka, E.J. Payton, D. Raabe, A. Kaysser-Pyzalla, G. Eggeler, Acta Mater. **59**, 1586–1600 (2011)
48. V. Raghavan, J. Phase Equilib. Diffus. **30**, 184–188 (2009)
49. A. Bouayad, Ch. Gerometta, A. Belkebir, A. Ambari, Mater. Sci. Eng., A **363**, 53–61 (2003)